Fuel 225 (2018) 26–34

Contents lists available at ScienceDirect

Fuel

journal homepage: www.elsevier.com/locate/fuel

Full Length Article

Coke from SARA fractions in VGO. Impact on Y zeolite acidity and physical properties

Jayson Fals, Juan Rafael García, Marisa Falco, Ulises Sedran*

Instituto de Investigaciones en Catálisis y Petroquímica INCAPE (UNL – CONICET), Colectora Ruta Nacional 168 km 0 – Paraje el Pozo, (3000) Santa Fe, Argentina

ARTICLE INFO

Keywords:
Catalytic cracking
Y zeolite
Intracrystalline mesoporosity
SARA fractions
Catalyst deactivation
Coke

ABSTRACT

The impact of the composition of the various hydrocarbon fractions in a conventional VGO (saturated SF, aromatic AF and resin RF) and the whole VGO on the coke formed in their catalytic cracking was evaluated over two Y zeolites with different degree of mesoporosity. The parent zeolite was in its protonic form, Si/Al relationship of 30 and the modified sample was desilicated by alkaline treatment. The fractions were separated from the VGO by means of ASTM D2007-11 method. The catalytic conversion experiments were performed in a batch, fluidized bed laboratory Riser Simulator reactor at 500 °C in the 0.7–3.0 s reaction time range, with a zeolite mass of 0.2 g and a zeolite/reactant mass of 1. Independent of zeolite, fraction SF was the easiest to crack. In the case of the AF fraction, the modified zeolite, with the highest intracrystalline mesoporosity, was more active than the parent zeolite. Gasoline was always the main product, with selectivities from 60 to 70%. All the feedstocks produced more coke on the modified zeolite; however, in spite of the higher coke yields, this zeolite suffered a lower loss of total acidity. As expected, a negative change in both acidity and textural properties (specific surface area and pore volume) were observed as a consequence of the formation of coke. The reactivity of VGO over both zeolites differed from that of fraction SF, even though it was the major fraction (68%). This behavior could be the consequence of interactions between the various fractions composing VGO.

1. Introduction

The catalytic cracking of hydrocarbons in transport fluidized bed reactors (FCC) is a well established process which converts low value, heavy molecular weight hydrocarbons, particularly vacuum gas oils (VGO) and also some residual cuts, into high value products such as gasoline, middle distillates, liquefied petroleum gas (LPG) and petrochemical olefins [1]. Conversions higher than 75 wt% are achieved in very short contact times [2]. Among many other issues, the characteristics of the feedstock are key factors in determining the overall process performance and the distribution of products [3,4].

Different hydrocarbon fractions can be distinguished in crude oils and their various constituting cuts. According to the solubility in diverse solvents with different polarities, at least four fractions can be separated from VGOs: saturated, aromatic, resin and asphaltenes, thus reflecting the SARA composition [5,6]. Paraffinic and naphthenic molecules with small amounts of heteroatoms mainly constitute the saturated fraction. It includes non-polar compounds such as linear, branched and cyclic hydrocarbons. The aromatic fraction is formed by aromatic cyclic hydrocarbons with one or more rings and moderate concentration of heteroatoms (particularly sulfur). Resins are, together with the asphaltene fraction, the heaviest fractions in crude, with high polarity and condensed aromatic structures. Particularly, asphaltenes comprise highly polar hydrocarbons, with condensed aromatic rings and alkenic side chains, plus heteroatoms such as sulfur, nitrogen, oxygen and metals included in the main structure [7,8].

The most used laboratory method to separate the SARA hydrocarbon fractions in a heavy feedstock is ASTM D2007-11 standard, which is performed over two chromatographic columns packed with clay and silica gel. Besides this classic method, there exist more sophisticated techniques, such as high performance liquid chromatography [9] and thin layer chromatography combined with flame ionization detection (FID) [7,10]. These methods are faster and consume lower amounts of solvents, as compared to chromatographic columns packed with silica and clay, but they are not completely reproducible [7].

FCC catalysts are composed, the main component being the Y zeolite, present in fresh catalysts from about 15 to 40 wt%, supported on a matrix (either active or inactive). Their acidity, considering amount, nature and strength, together with their textural properties are key factors in determining activity and selectivity in these catalysts. In that sense, it is important that reactant molecules diffuse as easily as

* Corresponding author.
E-mail addresses: jfals@fiq.unl.edu.ar (J. Fals), jgarcia@fiq.unl.edu.ar (J.R. García), mfalco@fiq.unl.edu.ar (M. Falco), usedran@fiq.unl.edu.ar (U. Sedran).

https://doi.org/10.1016/j.fuel.2018.02.180
Received 17 December 2017; Received in revised form 19 February 2018; Accepted 28 February 2018

possible through the catalyst pore system until reaching the active sites which are to catalyze the chemical reactions through carbocation mechanisms [11]; obviously, products are subjected to the same diffusion circumstances.

Even though Y zeolite has been used through decades given its excellent activity, selectivity and hydrothermal stability, the microscopic nature of its pore system imposes severe diffusion restrictions to bulky reactants and products, which condition their interaction with acidic active sites [12–14]. A possible solution to this fact could be provided by the generation of intracrystalline mesoporosity in the zeolite, alkaline lixiviation being a simple technique which selectively removes silicon atoms from the crystalline network, thus producing a partial destruction of the network leading to interconnected mesopores [15–19].

An additional issue, intrinsic to acidic zeolites facing hydrocarbons at high temperatures, is derived from the fast deactivation the catalysts must tolerate from the deposition of coke. The complex set of chemical reactions taking place in FCC inevitably leads to coke deposition, which has a twofold impact: active acid sites are covered and pore blocking is also observed [20–22]. Both coke yield and nature (H/C relationship, condensation degree) will depend on the composition of the feedstock, the catalyst properties and process conditions. Thus, they could affect the delicate heat balance of the commercial units, based on the combustion of coke in the regeneration section to provide the heat consumed by the overall endothermic set of reactions in the riser [23].

Ibarra et al. [24] studied coke deactivation mechanisms during the catalytic cracking of different feedstocks under FCC conditions, using various techniques such as Fourier transformed infrared (FTIR) spectroscopy, temperature programmed oxidation coupled with FTIR spectroscopy and mass spectrometry (TPO-FTIR and TPO-MS), ^{13}C coupled polarized magic angle spinning nuclear magnetic resonance (CP-MAS NMR), X-ray photo spectroscopy (XPS), Raman spectroscopy and matrix assisted laser desorption ionization time of flight mass spectrometry (MALDI-TOF MS). They digested the inorganic portion of the samples to obtain two coke fractions, respectively soluble and insoluble in dichloromethane, and further analyzed them. Two main types of coke were observed, one of them with strong aromatic character and low H/C relationship, constituted by condensed aromatic rings, the other one showing olefinic nature, constituted by species with conjugated double bonds [24].

Given feedstock, catalyst and process conditions, it is important to know the reactivity of the VGO, which certainly reflects that of its constitutive SARA fractions, to recognize, and ideally predict and understand, their impact on the process yields and product quality, as well as on catalyst performance. It is the objective of this study to crack a VGO feedstock and the fractions constituting it over Y zeolites with different degree of intracrystalline mesoporosity in order to estimate their individual impact on the catalyst properties after coke formation. As already mentioned, FCC catalysts are compound, with Y zeolite exclusively contributing the micropore specific surface area and most of the acidic function in the particles, while the matrix usually plays important roles such as support, heat carrier, and zeolite dilution media [12,25]. Given that the main aim in this work is to evaluate the impact of coke formation on the deactivation of the zeolite component in FCC catalyst (both losses in acidity and changes in textural properties), the catalytic activity was observed only in the steamed zeolites, to avoid the influence of the matrix and binder. Moreover, the dilution effect could be significant.

2. Experimental

2.1. SARA VGO fractioning

A paraffinic vacuum gas oil was fractionated into its SARA fractions by means of ASTM D2007-11 standard [26]. The properties of the parent VGO are shown in Table 1.

Initially, the asphaltene fraction was precipitated with *n*-pentane (Merck, > 99.5 wt%), and the remaining oil was further passed through glass chromatographic columns using a series of solvents with increasing polarities. Two columns were used in series, each having 310 mm length and 44 mm diameter. The upper column was loaded with 50–500 μm Attapulgite clay particles to adsorb polar compounds and resins (resin fraction, RF). The lower column was loaded with 63–200 μm silica gel particles (Merck, Silica gel 60, code number 107734) which is aimed at retaining the aromatic fraction. The columns were swept with *n*-pentane to elute the saturate fraction (SF) and then separated. The upper column, containing the RF fraction was washed with a acetone:toluene 50:50 vol mixture to remove resins from the bed. The lower column was rinsed with toluene and aromatic compounds (AF fraction) were collected. All the fractions were dried with anhydrous $CaCl_2$ (Merck, > 99.9 wt%) and finally the solvents in each fraction were removed in a rotatory vacuum evaporator at 40 °C and 417 Torr. The complete removal of solvent in each fraction after treatment was confirmed by means of GC analysis.

Table 1
VGO properties.

°API	22.94
Aniline point (°C)	80.1
CCR (wt.%)[a]	0.11
Distillation curve (°C)[b]	
Initial	199
10% vol.	345
30% vol.	405
50% vol.	438
70% vol.	465
90% vol.	495
Final	512
Nickel (ppm)	0.10
Vanadium (ppm)	0.73
Sodium (ppm)	0.38
Iron (ppm)	2.36
Copper (ppm)	< 0.02
Sulphur (wt.%)	0.39

[a] ASTM D-4530.
[b] ASTM D-1160.

2.2. Alkaline treatment of Y zeolite

Two Y zeolites with different degrees of intracrystalline mesoporosity were used. The parent zeolite was a commercial Y zeolite (CBV 760, Zeolyst International, protonic form). The modified sample was the result of the following alkaline treatment on the parent zeolite [14,27–29]. 10 g of zeolite were suspended in 300 mL of a NaOH solution (0.10 M) and the suspension was stirred during 15 min at room temperature. Then, a 1.00 M HCl solution was added to the suspension to reach a final pH of 2.00 in order to quench the alkaline leaching. The thus desilicated zeolite was separated from the solution by filtration and submitted to three cycles of ion exchange using 5 mL of 0.50 M NH_4Cl solution per gram of zeolite. The ion-exchanged zeolite was then thoroughly washed using deionized water, dried in an oven during 16 h at 110 °C and finally calcined in a muffle oven during 4 h at 550 °C in order to obtain the zeolite in its acid form. The parent and desilicated zeolites were named Y-00 and Y-10, respectively. Both the modified and untreated zeolites were hydrothermally stabilized by steaming during 5 h at 788 °C (100% steam). The steamed zeolites were named Y-00-S and Y-10-S, respectively, in concordance with their parent zeolites.

2.3. Physicochemical characterization

The textural properties of the zeolites, both before and after reaction (coked samples), were assessed by means of nitrogen adsorption at −196 °C using a Micromeritics ASAP 2020 sorptometer. Before analysis, the samples were degassed under vacuum during 3 h at 300 °C.

The BET model (Brunauer-Emmet-Teller) was used in the $0.005 < P/Po < 0.030$ range in order to determine the specific surface area. The total pore volume was assessed using the amount of nitrogen adsorbed until $P/Po \sim 0.98$. The micropore volume and the mesopore specific surface area were estimated with the *t*-plot method, considering 3.5 Å < *t* < 5.0 Å. The BJH model (Barrett-Joyner-Halenda) was used in order to determine the mesopore size distribution and the average mesopore diameter.

Both fresh and coked zeolites were analyzed by Fourier transform infrared spectroscopy analysis. Self-supporting wafers (440 g/m^2) were formed by pressing 100 mg of zeolite at 1 ton/cm^2, which were placed in a cell with CaF_2 windows. The samples were initially outgassed under vacuum (about 10^{-4} Torr) during 2 h at 450 °C and, after cooling down to room temperature, a background spectrum was recorded in a Shimadzu FTIR Prestige-21 spectrophotometer. The background spectra gathered over the coked catalysts were used in order to elucidate the nature of carbonaceous deposits. The signal at 1580 cm^{-1} was assigned to "aromatic type" coke meanwhile a signal at 1610 cm^{-1} was attributed to "olefinic type" coke [30,31]. The acidic properties of both the fresh and coked zeolites, that is, the residual acidity in the latter case, were determined by using pyridine (Py) as a probe molecule. Pyridine (Merck, 99.5 wt%) was adsorbed at room temperature and, after successive desorptions steps at 150, 300 and 400 °C and 10^{-4} Torr, spectra were collected at room temperature in the range of 1700 to 1400 cm^{-1} with a resolution of 4 cm^{-1}. The amounts of Brönsted and Lewis acid sites were calculated from the integrated absorbance of the bands at 1545 cm^{-1} and 1450–1460 cm^{-1}, respectively, by using the integrated molar extinction coefficients reported in the literature [32].

A Shimadzu XD-D1 diffractometer with Cu Kα radiation operating at 30 kV and 40 mA was used in order to evaluate the X-ray diffraction (XRD) patterns of the different zeolites. The XRD patterns were gathered in the $5^\circ < 2\theta < 40^\circ$ range and the unit cell sizes (UCS) and the crystallinities were calculated according to ASTM D-3942 and ASTM D-3906 standards, respectively. The Si/Al atomic relationship in the framework of the different zeolites were estimated according to the Breck-Flanigen's correlation [33].

2.4. Catalysts and evaluation tests

The catalytic experiments were performed in a batch, fluidized bed laboratory unit with internal recirculation, the CREC Riser Simulator reactor, which was specifically designed to mimic the conditions of the commercial FCC process [34]. A comprehensive description of the unit can be found elsewhere [34–36]. The conversion experiments at different reaction times were performed using a conventional FCC VGO feedstock, whose properties are shown in Table 1, and its most abundant fractions (SF and AF). Moreover, some experiments were also performed with the resin fraction (RF), so as to observe the contributions that this fraction may exert. In order to avoid excessive amount of coke on catalyst and a total loss of acidity in the zeolites the reaction time in the experiments was very short (0.7, 1.5 and 3.0 s). The CREC Riser Simulator reactor is appropriate to operate under very short reaction times and its fluidized catalyst bed allows for a more efficient catalyst-reactants contact, thus avoiding the high coke yields observed in fixed bed reactors [37]. The reaction temperature was 500 °C and the zeolite to oil mass relationship was 1.0, achieved with 0.2 g of zeolite in all the cases. The reaction products were analyzed by means of on-line capillary gas chromatography, using a 30 m long, 250 μm diameter and 0.25 μm film thickness, non-polar, dimethylpolysiloxane column. The content of coke on the zeolites was assessed following a temperature programmed oxidation method, which consists in burning-off the carbonaceous deposits and converting the carbon oxides formed into methane over a Ni catalyst, which was quantified with the help of a FID detector. In all the experiments, the mass balances (recoveries) closed to more than 90 wt%.

Table 2
Textural and crystalline properties of parent and modified zeolites before and after steaming.

	Zeolite			
	Y-00	Y-10	Y-00-S	Y-10-S
Textural properties				
BET specific surface area (m^2/g)	1038	919	582	538
Micropore specific surface area (m^2/g)[a]	925	649	442	386
Mesopore specific surface area (m^2/g)	113	270	140	152
Total pore volume (cm^3/g)	0.63	0.62	0.47	0.55
Micropore volume (cm^3/g)	0.40	0.26	0.24	0.16
Mesopore volume (cm^3/g)[a]	0.23	0.36	0.23	0.39
Average mesopore diameter (Å)	23	26	104	113
Crystalline properties				
Crystallinity (%)	100[b]	75	90	67
Unit cell size (Å)	24.24	24.25	24.24	24.21
Si/Al in the framework[c]	33.0	27.3	33.0	86.7

[a] Micropore surface area = BET specific surface area − Mesopore surface area. Mesopore volume = Total pore volume − Micropore volume.
[b] Reference sample.
[c] Calculated according to the Breck-Flanigen's correlation [33].

3. Results and discussion

3.1. SARA fractions in VGO

The efficiency of the SARA fractionation method was very high, with 99.14% recovery. The saturated fraction SF represented 68.12 wt % in VGO, thus confirming its paraffinic nature, in accordance with its high aniline point (see Table 1) [2]. The second most abundant fraction was that of aromatics AF, with a yield of 19.90 wt%, followed by the resin fraction RF with 10.31 wt% and the very minor existence of the asphaltene fraction AsF with only 0.81 wt%. The GC analysis of the most abundant fraction (SF) showed that predominant *n*-paraffins had between 12 and 40 carbon atoms per molecule.

3.2. Zeolite properties

Table 2 shows the textural and crystalline properties of the parent and modified zeolites, both before and after the hydrothermal stabilization step. The effect of the various desilication experimental parameters on the porous structure of the Y zeolite has been the object of a significant number of studies which can be consulted in the literature [13,14,17,19,28,38]. However, in order to correlate the catalytic performances with these physical properties, a brief discussion is performed on the results.

It is interesting to note that the parent zeolite was a commercial CBV 760 zeolite (Y-00) which already had mesopores derived from its manufacturing process, in order to achieve its high Si/Al ratio. The parent zeolite is an ultrastable (USY) one, with a higher structural resistance. As expected, the alkaline treatment increased mesoporosity in the zeolite, reflected in both the mesopore volume (0.23 cm^3/g in zeolite Y-00, 0.36 cm^3/g in zeolite Y-10) and the mesopore specific surface area (113 and 270 m^2/g, respectively). Moreover, the average diameter in mesopores increased from 23 to 26 Å. Simultaneously, a loss of microporosity was observed, a fact which is directly associated to the 25% loss of crystallinity in zeolite Y-00 after desilication [39].

Steaming the zeolites led to expected results; that is, it produced a loss of crystallinity and specific surface area, which was more intense on desilicated sample (Y-10). However, all the properties (specific surface area, mesoporosity, average mesopore size, and crystallinity) maintained the trends observed with the zeolites before steaming. Similar results had been reported by Martínez et al. [13] after steaming Y zeolites treated with NaOH and EDTA. UCS in the parent zeolite Y-00 did not change after steaming, probably due to the previous

Table 3
Brönsted (B) and Lewis (L) acid site concentrations (μmol Py/g) in zeolites Y-00-S and Y-10-S.

	Zeolite					
	Y-00-S			Y-10-S		
Acidity	B	L	B/L	B	L	B/L
T_{des}: 150 °C	5.6	35.2	0.16	13.1	55.8	0.23
T_{des}: 300 °C	3.4	26.3	0.13	10.3	32.4	0.32
T_{des}: 400 °C	2.4	15.2	0.16	3.2	18.5	0.17

ultrastabilization treatment. However, the partial destabilization of the crystalline network during desilication in zeolite Y-10 eased a significant dealumination during steaming.

Table 3 shows the distribution of acidic sites in the parent and modified zeolites after hydrothermal stabilization, according to their nature and acid strength. It can be seen that, even though the Brönsted to Lewis (B/L) relationship after desorptions at 400 °C (corresponding to strong acid sites) were essentially the same for both zeolites, both Brönsted and Lewis sites were present at higher concentrations in the modified Y-10-S zeolite if the absolute acidities (μmol Py/g) are compared. The difference between samples was relatively more significant in reference to Brönsted sites; for example, the total amount of Brönsted acidity, as given by the desorption at 150 °C, changed from 5.6 to 13.1 μmol/g. A similar trend was observed after desorbing pyridine at higher temperatures, given that the B/L relationship was higher in the Y-10-S zeolite than that of the Y-00-S sample. It has been postulated that the process of lixiviation with alkaline solutions can be made selective to remove silicon from the zeolite crystalline network, thus inducing a decrease in the Si/Al relationship and increasing the amount of acidic sites (mass basis) [19,38]. Moreover, an increase in the number of Lewis sites after desilication was also observed, in accordance with previous reports [28,38,40,41]. This can be assigned to the fact that part of the aluminum atoms originally present in the network is also leached out and further deposited as amorphous material, taking part of extra-framework aluminum species with certain acidic character [29,38].

3.3. Catalytic performance

The reactivity of a given hydrocarbon feedstock over an acidic catalyst depends on how the molecules composing it can form carbocations, in turn a function of the structural and chemical characteristics of the molecules [42–44]. For example, Stratiev et al. [45] cracked eleven VGOs with different compositions and found a linear correlation between the yields of the various products and the content of hydrogen in each feedstock. This correlation is useful to estimate the maximum expected conversion, provided the content of hydrogen in the feedstock is known [45].

As it was show in Section *3.1. SARA fractions in VGO*, the saturated (SF) and aromatic (AF) fractions represented more than 88% of the whole VGO. Then, the catalytic experiments at different reaction times were performed using the parent, conventional VGO and those main fractions. Moreover, some experiments at a fixed time were performed with the resin fraction (RF), whose proportion in the VGO was 11 wt%. Conversion was defined as the typical one in FCC, accounting for the yields of dry gas (DG, C1-C2), liquefied petroleum gas (LPG, C3-C4), gasoline (C5-216 °C) and coke, each of them calculated as the relationship between the mass of the corresponding product and the mass of feedstock injected in each experiment.

Fig. 1 shows the conversions of the VGO and the various fractions observed on each zeolite as a function of reaction time. It can be seen with the aromatic fraction that the activity of the modified zeolite was higher. This behavior could be attributed to the higher intracrystalline mesoporosity and density of acid sites in zeolite Y-10-S (see Tables 2 and 3). The increased intracrystalline mesoporosity favors the diffusion transport of the bulky molecules present in the aromatic fraction, thus improving the access to the active sites for cracking [14,19,28]. Conversely, when the saturated fraction was cracked, a higher activity was observed with the non-desilicated zeolite (Y-00-S). This is probably due to its higher microporosity which would preferentially favor the transport of saturated molecules as compared to aromatics and VGO. This fact is particularly true given the high proportion of *n*-paraffins present in SF fraction. García et al. [28] reported a detailed analysis of the impact of the molecular size of various compounds in the catalytic upgrading of bio-oil from pine over FCC catalyst prototypes based on zeolites with different degree of intracrystalline mesoporosity. It was observed that the higher the intracrystalline mesoporosity, the more significant the conversion of aromatic ethers and bulky phenolic compounds, as the consequence of easier access to the active acidic sites. On the contrary, to those oxygenated compounds with smaller molecular size, such as furfural, whose conversion would not be very sensitive to pore size, converted more extensively on zeolites with lower intracrystalline mesoporosity, thus supporting the hypothesis that its conversion is more dependent on zeolite crystallinity rather than on mesoporosity [28]. Concerning VGO, its conversion on the desilicated zeolite was slightly higher, showing an intermediate behavior between the saturated and aromatic fractions. The conversion of the resin fraction over both zeolites showed to be similar to that of the aromatic fraction.

Its also reported in previous studies about the reactivity of the different SARA fractions in an atmospheric tower residue under FCC conditions, the reactivity of the individual fractions in the cut is not additive [43], a condition attributed to interactions among the various fractions when composing the whole feedstock.

Table 4 shows the selectivities to the different hydrocarbon cuts typical in FCC, obtained in the catalytic cracking of VGO, SF, AF and RF at the same conversion. Gasoline was always the most important product, with selectivities between 60 and 70 wt%, followed by gases (DG and LPG). VGO and RF fraction were the feedstocks with the highest gasoline yields. The high gasoline yield from the RF fraction as compared to those from the other fractions has been previously observed in the catalytic cracking of the various fractions in an ATR atmospheric resid [43].

In relation to the composition of the gasoline cut, both AF and RF fractions showed a higher selectivity to aromatic hydrocarbons (between 33 and 44% wt.) over both catalysts. Even though dealkylation of aromatic hydrocarbons with important side chains in fractions AF and RF may produce linear fragments, a higher selectivity to aromatic compounds is to be expected starting from these fractions [43]. The saturated fraction showed a higher selectivity to aliphatic hydrocarbons (*n*-paraffins, *i*-paraffins, olefins and naphthenes). In the comparison between zeolites, it can be seen that the modified simple (Y-10-S) favored the yield of aromatic compounds when the different fractions were used.

It can be seen in the comparison of selectivities of the various groups over both zeolites that the saturated fraction SF produced the highest dry gas yields. This characteristic could be based on the cracking of long chains in open molecules and side chains in cyclic compounds. On the contrary, the resin fraction showed the lowest yields to gases (mainly dry gas), particularly on the modified zeolite. This can be because the higher mesoporosity in the lixiviated zeolite improves the diffusion of the primary product gasoline, thus decreasing the possibility of overcracking to lighter products.

3.3.1. Coke yield

Carbonaceous deposits on FCC catalysts are the reason for their fast, reversible deactivation and, simultaneously, the heat source to sustain chemical reactions in the riser reactor when burnt off in the regenerator. The nature of the feedstock, operational conditions and

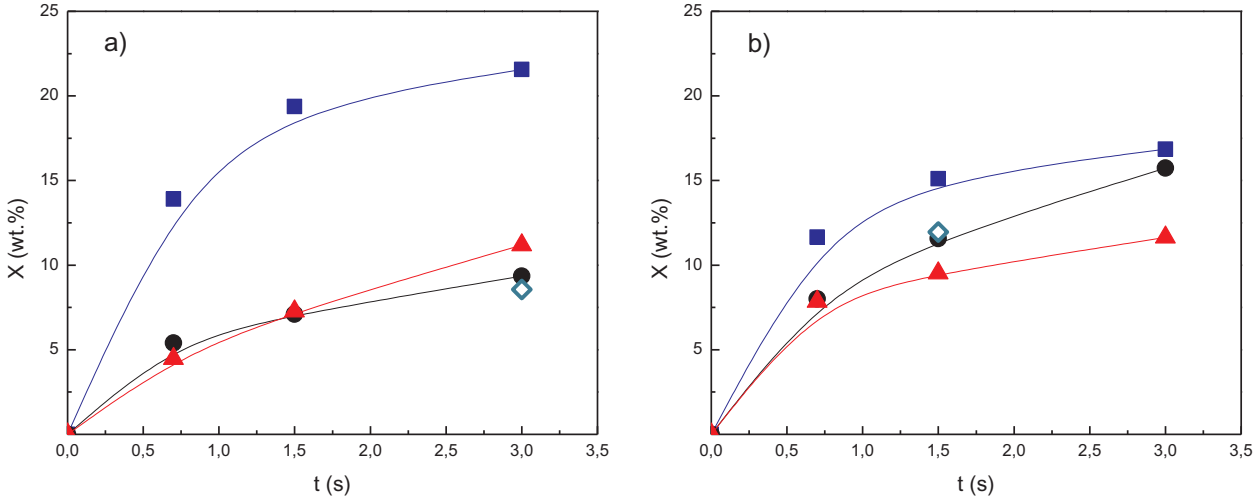

Fig. 1. Conversion of VGO and SF, AF and RF fractions as a function of reaction time at 500 °C over zeolites (a) Y-00-S and (b) Y-10-S. Symbols: *triangles*, *VGO*; *squares*, SF; ●, AF; *open diamonds*, RF.

Table 4
Product selectivities in the conversion of VGO, SF, AF and RF feedstocks over zeolites Y-00-S and Y-10-S (conversions approximately 11 wt%).

	Y-00-S				Y-10-S			
	VGO	SF	AF	RF	VGO	SF	AF	RF
S_{DG} (wt.%)	15.08	18.37	17.75	13.17	15.57	16.21	16.09	11.68
S_{LPG} (wt.%)	10.35	15.11	10.98	12.37	10.27	14.63	16.83	11.70
$S_{gasoline}$ (wt.%)	69.85	64.96	68.11	69.18	66.68	66.65	60.19	68.60
Gasoline composition (%)								
n-Paraffins	12.0	9.1	10.4	11.3	7.0	10.4	13.7	13.0
i-Paraffins	9.5	5.4	17.1	17.3	9.2	8.4	6.9	2.0
Olefins	28.2	38.5	31.5	29.6	34.6	40.3	21.1	27.5
Naphthenes	13.9	19.4	11.1	8.3	14.8	10.1	16.7	13.8
Aromatics	36.4	27.0	30.1	33.4	34.3	30.9	41.7	43.6
S_{coke} (wt.%)	4.47	1.49	3.07	5.17	7.25	2.43	6.59	7.65

catalyst properties all condition coke yield and characteristics. The CCR index indicates the coke forming trend of a given hydrocarbon cut, but it is not possible to directly associate it with feedstock composition. It is to be expected the CCR number of the parent feedstock will distribute among the various fractions after fractionation, but the resulting individual CCRs should not be expected to follow an additive relationship. Usually, heavy molecular weight hydrocarbons with condensed aromatic structures are considered the most significant precursors in the formation of coke in FCC [46].

Fig. 2 shows coke yields as a function of reaction time for VGO, SF and AF feedstocks over the two zeolites, where it can be seen that the coke yields from VGO and AF approximately doubled that from SF fraction. The compound feedstock VGO essentially followed the behavior of AF fraction, besides it contains 68 wt% of saturated compounds, thus showing the strong non-additive behavior of its constitutive fractions. This would suggest a possible interaction among the various fractions composing VGO. Isolated experiments with the resin RF fraction yielded 0.6 wt% coke in the case of zeolite Y-00-S and 0.8 wt% in the case of Y-10-S zeolite at similar conversions of about 11 wt%. Pujro et al. [43] observed that the resin fraction in an atmospheric tower resid was the one yielding more coke over commercial FCC catalysts.

Independent from the feedstock, the modified zeolite Y-10-S produced more coke than the parent zeolite. The ability of zeolites with increased intracrystalline mesoporosity to form more coke has been noticed in studies with different complex feedstocks such as VGO, ATR-VGO and pine and maple bio-oils [19,28,47,48], which has been attributed to the higher free volume available in mesopore cavities. This allows accommodating coke precursors more easily as well as favoring oligomerization, alkylation, cyclization, hydrogen transfer and condensation reactions leading to the formation of coke deposits [47,48].

It is to be noted that albeit zeolite Y-10-S showed the highest coke yields, even at very short reaction times, it maintained its higher activity as compared to zeolite Y-00-S in converting VGO and AF feedstocks (see Fig. 1). This relatively higher resistance to coke deactivation shown by zeolites with intracrystalline mesoporosity has been noticed by other authors in the methanol to gasoline (MTG) process [49,50], which was assigned to the interconnectivity between intracrystalline mesopores avoiding pore blocking by coke. Moreover, it has been concluded that mesoporosity improves the diffusion of bulky coke precursor molecules out of the zeolite structure [49]. This would explain that the modified zeolite keeps higher activity in spite of its higher coke yield.

3.4. Coke nature

Fig. 3 shows the combustion profiles of the coke formed from feedstocks VGO, SF, AF and RF over both zeolites, conversion being approximately 11 wt%. A major combustion peak was observed in cracking all feedstocks at temperatures higher than 600 °C for the case of zeolite Y-00-S, and between 500 and 600 °C for zeolite Y-10-S. Moreover, a shoulder can be seen at about 330 °C in all the cases; independent of feedstock, the proportion of that shoulder in reference to the total area under the combustion profiles was the highest in zeolite Y-00-S. These distinctive behaviors suggest the nature of the coke is not the same on both zeolites, as it will be discussed later. Previous studies report that combustion peaks at low temperatures in the 300–350 °C range are due to the removal of aliphatic compounds and the initial combustion of dienes and aromatic structures with a relatively high H/C relationship [24]. The coke burnt off at temperatures higher than 500 °C is associated to the condensation of diene and aromatic structures with low H/C relationship. This second type of coke originates in the zeolite micropores but, given its high degree of condensation, it has been postulated that the further growing is promoted outside the zeolite crystals [24,51].

Substantial differences between the temperatures at which the coke combustion rate is maximum over each zeolite can be appreciated for feedstocks VGO and SF. In the case of VGO, the peak was located at 660 °C for zeolite Y-00-S, while the temperature was 515 °C for zeolite Y-10-S. In the case of fraction SF, the corresponding temperatures were 627 and 550 °C, respectively. The shift to lower temperatures in the

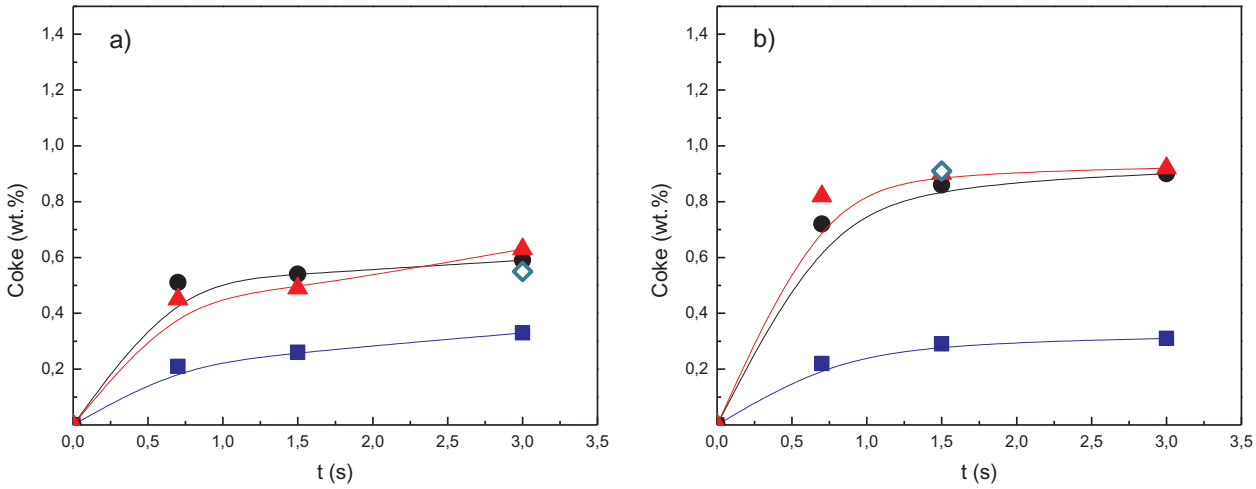

Fig. 2. Coke yields in the cracking of VGO and SF, AF and RF fractions as a function of reaction time at 500 °C over zeolites (a) Y-00-S and (b) Y-10-S. Symbols: *triangles*, *VGO*; *squares*, SF; ●, AF; *open diamonds*, RF.

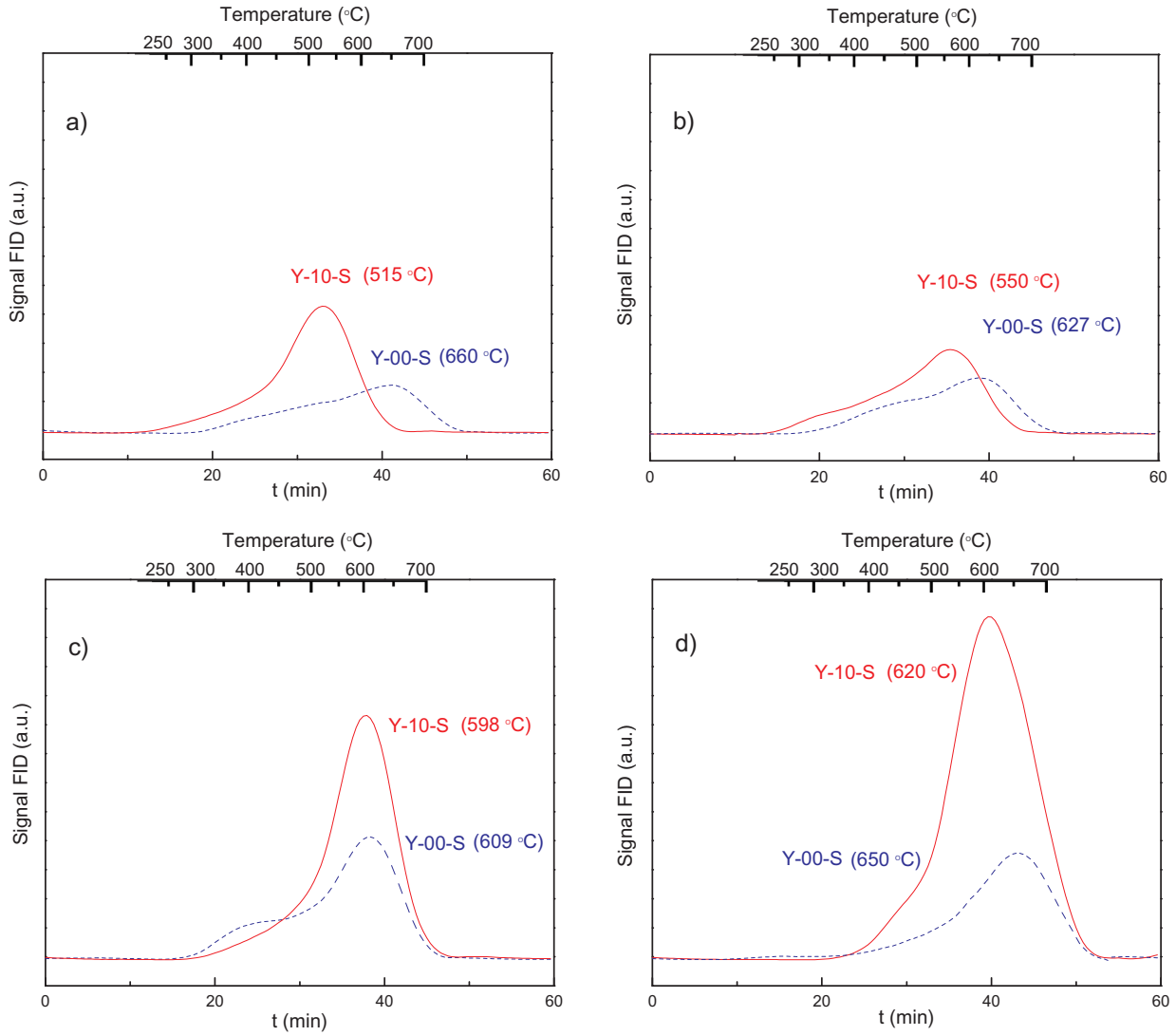

Fig. 3. Combustion profiles (TPO) of the coke formed in the cracking of (a) VGO, (b) SF, (c) AF and (d) RF fractions. Conversion approximately 11 wt%.

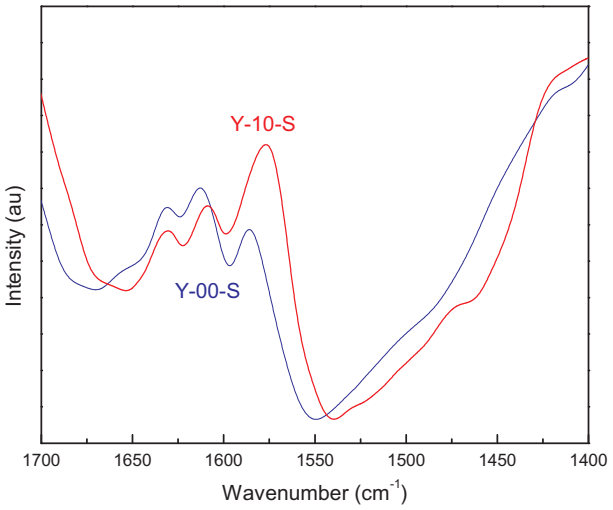

Fig. 4. Example FTIR spectra of the zeolites coked during the conversion of the aromatic fraction. Conversion approximately 11 wt%.

Table 5
Textural properties of the parent and modified fresh and coked zeolites used in the cracking of the various feeds (conversion approximately 11% wt.).

	Y-00-S				Y-10-S			
	Fresh	VGO	SF	AF	Fresh	VGO	SF	AF
BET specific surface area (m^2/g)	582	464	490	415	538	473	509	449
Micropore specific surface area (m^2/g)[a]	442	411	416	355	386	357	366	326
Mesopore specific surface area (m^2/g)	140	53	74	60	152	116	143	123
Total pore volume (cm^3/g)	0.47	0.30	0.32	0.29	0.55	0.40	0.45	0.38
Micropore volume (cm^3/g)	0.24	0.17	0.16	0.13	0.16	0.13	0.16	0.14
Mesopore volume (cm^3/g)[a]	0.23	0.13	0.16	0.16	0.39	0.27	0.29	0.24
Average mesopore diameter (Å)	104	96.0	97.7	94.0	113	102	104	100

[a] Micropore surface area = BET specific surface area − Mesopore surface area. Mesopore volume = Total pore volume − Micropore volume.

peaks' location in case of using the desilicated zeolite had been observed in the cracking of other feedstocks from fossil sources (VGO and ATR-VGO mixtures, [19]) and also in the catalytic upgrading of pine sawdust bio-oil [28]. It is widely accepted that coke in FCC catalysts accumulates in the mesopores (either in the matrix or in the zeolite intracrystalline mesoporosity formed during equilibration). This coke consists in polyaromatic domains which are heterogeneously distributed and also includes trapped molecules of saturated hydrocarbons [21]. Analogously, it could be accepted that the higher mesopore volume in zeolite Y-10-S, allows retaining a higher proportion of saturated molecules in coke as compared to zeolite Y-00-S, thus resulting in a less condensed coke which combust at lower temperatures [52]. Given that fractions AF and RF contain lower concentrations of saturated molecules than fraction SF, this effect is less notorious on the coke they formed, and the shift in the combustion peak maxima was only 11 and 30 °C, respectively.

Ibarra et al. [24] characterized the coke deposits on an equilibrium FCC catalyst after cracking VGO, bio-oil and their mixtures, by means of FTIR. They attributed the various bands to different chemical functionalities. Particularly, two characteristics signals were observed: one at 1580 cm^{-1}, which was assigned to "aromatic type" coke, where condensed aromatic rings prevailed, and another one at 1610 cm^{-1}, which was assigned to "olefinic type" coke, mainly composed by compounds with conjugated double bonds [30,31]. Fig. 4 shows example FTIR spectra of the zeolites coked during the conversion of the aromatic fraction. The same bands were also present with all the other feedstocks, differences being observed only in intensity. Three characteristic bands were noticed, corresponding to the two types of coke mentioned (1580 cm^{-1}, aromatic coke; 1610 cm^{-1}, olefinic coke) and that attributed to conjugated olefins at 1630 cm^{-1} [53].

Fig. 5 shows the intensities of the bands at 1580 and 1610 cm^{-1} observed on the zeolites after cracking VGO, SF, AF and RF feedstocks. Independent from the feedstock, the parent zeolite Y-00-S exhibited, predominantly, the signal at 1610 cm^{-1} (olefinic coke). These results are consistent with the combustion profiles shown in Fig. 3, where a higher contribution from the shoulder at lower temperatures (300 °C) was observed in simple Y-00-S; the shoulder could be attributed to the combustion of olefinic coke, with higher H/C relationship [52]. The relative intensities of both bands observed in the modified zeolite Y-10-S, with higher intracrystalline mesoporosity, corresponded to the nature of the feedstock in each case. Thus, when the saturated fraction SF was converted, the signal associated to olefinic coke (1610 cm^{-1}) prevailed and, when the aromatic and resin fractions were the reactants, that of aromatic coke (1580 cm^{-1}) prevailed. In the case of VGO, its paraffinic character was reflected into the preponderance of the signal corresponding to olefinic coke.

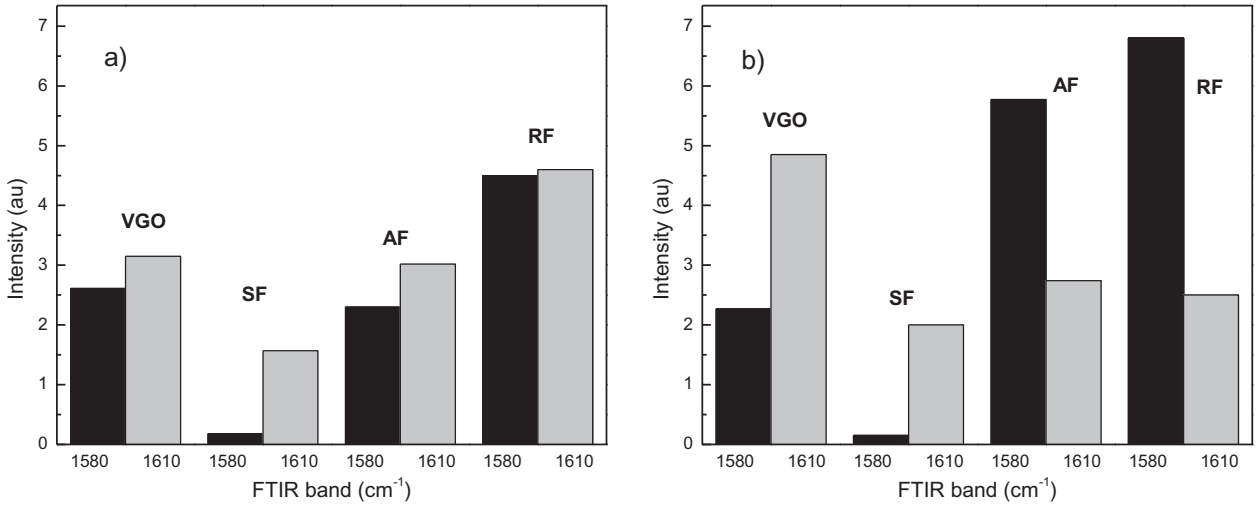

Fig. 5. Intensities of the FTIR bands assigned to aromatic coke (1580 cm^{-1}) and olefinic coke (1610 cm^{-1}) formed in the conversion of VGO and AF, SF and RF fractions at 500 °C on zeolites (a) Y-00-S and (b) Y-10-S. Conversion approximately 11 wt%.

3.5. Changes in catalyst properties after coke formation

Table 5 shows the changes in the textural properties of both zeolites after reaction. It was observed in all the cases that both the specific surface areas (BET, micro and mesopore surface area) and pore volumes (total, micro and mesopore volume) decreased in comparison to the fresh samples. Moreover, the average mesopore sizes, calculated according to the BJH method, were smaller in the coked zeolites, thus suggesting a partial pore blocking process occurred. The losses in the total specific surface area were up to 25% in zeolite Y-00-S and up to 15% in zeolite Y-10-S. The reductions in total pore volume were up to 38 and 31%, respectively. In general terms, in both zeolites, mesoporosity was relatively more affected than microporosity, an observation which is consistent with the analysis about coke formation in relation to results in Fig. 3. In effect, the predominance of coke burnt off at temperatures higher than 500 °C (associated to aromatic compounds), can be seen. That coke has been postulated to be developed outside the zeolite crystals, i.e., in the intracrystalline mesopores of the zeolites [24,48]. The relative magnitudes of the impact of the various feedstocks on the physical properties (specific surface area and pore volume) of the zeolites was the same in both catalysts: SF < VGO < AF. This can be attributed to the higher concentration of polyaromatic molecules in VGO and AF, which are strong contributors to coke formation, and the consequently higher coke yields. The modified zeolite (Y-10-S) showed less significant changes in its properties as a consequence of the coke formation on its surface, which could be assigned to the increased interconnectivity in mesopores [49,50]. This fact is also the reason for the comparatively higher activity in cracking VGO and AF feedstocks (see Figs. 1 and 2), as already discussed.

As it is well known, a critical property in this type of catalysts is their acidity (nature, density, strength), given the carbocationic reaction mechanism governing the chemical processes and, consequently, activity and selectivity [11,54]. The impact of coke on the acidic sites should reflect in a decrease in their density and consequently catalyst activity [55–57]. Fig. 6 shows the amount of total acidity (Brönsted and Lewis sites after the desorption of pyridine at 150 °C) in both zeolites, both at the fresh and coked states after conversion of the various feedstocks. Values between brackets indicate the corresponding coke yields.

As expected, acidity was lower in all the coked samples, as compared to the fresh zeolites, losses being higher than 40% in all the cases, even though conversion and coke yields were low. The ranking of coke yields at approximately the same conversion (11%) was: SF < AF < VGO. The higher impact of coke from the aromatic fraction on catalyst acidity (it implies a lower residual acidity) could be due

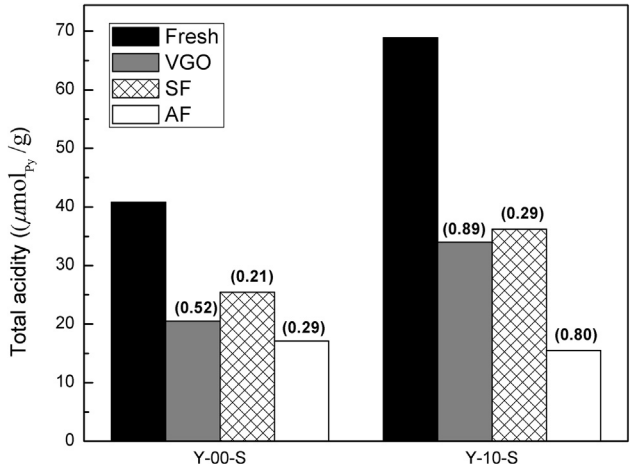

Fig. 6. Total acidity (Brönsted + Lewis) of the fresh and coked zeolites used in the cracking of the various feeds (conversion approximately 11 wt%). Values between brackets indicate coke yields.

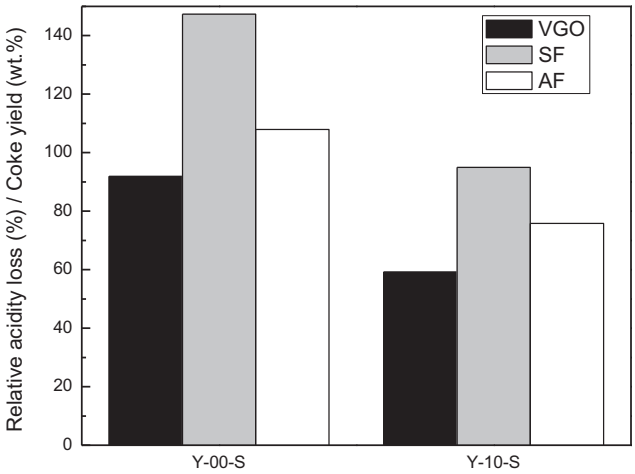

Fig. 7. Relative acidity loss per unit coke yield of the fresh and coked zeolites used in the cracking of the various feeds.

to the molecules with resonant structures and high electronic density, which confers them a neat basic character and strong affinity for the acidic sites. On the contrary, fraction SF, containing mainly saturated hydrocarbons, with lower basic character, was the feedstock with the minimum impact on acidity. VGO showed a behavior intermediate to those of the AF and SF fractions in relation to deactivation, even though coke selectivity was higher (see Table 4).

It was noticed that the aromatic fraction AF reduced 63% of the total acidity in zeolite Y-00-S and 77% in zeolite Y-10-S, particularly affecting Lewis acidity. The concept that, in highly crystalline zeolites, Lewis sites are somehow hidden in the structure [58], could be taken into account to understand that the more significant relative decrease of acidity in zeolite Y-10-S could be due to the higher accessibility to the active sites by molecules in the aromatic fraction, and consequent higher coke formation. This is consistent with the previous discussion about the notable predominance of aromatic-type coke (1580 cm^{-1} band in the FTIR spectrum) which was deposited on zeolite Y-10-S during the conversion of AF fraction (see Fig. 5).

Fig. 7 shows the loss in acidity in both catalyst samples relative to coke yields after cracking VGO, SF and AF feedstocks. It can be seen that in both cases the SF fraction produced the highest decrease in acidity per unit mass of coke followed by the fraction AF and finally VGO. The higher impact of SF on the acidic function can be attributed to the easier access of molecules in the fraction to the acidic sites and, consequently, coke formed from this fraction covers a higher proportion of acid sites. On the other hand, molecules in the aromatic fraction have lower accessibility to the acid sites and their coke affects them to a lower extent, because it is formed essentially outside the zeolite crystals [45]. The parent zeolite showed higher acidity losses, referred to coke yield, as compared to the desilicated zeolite. These results are consistent with the higher loss in specific surface area, both in micropores and mesopores (see Table 5).

4. Conclusions

The reactivity of the various fractions comprising a paraffinic VGO over zeolites with different intracrystalline mesoporosity as well their impact on acid and textural properties were studied after separating them by means of ASTM D2007-11 standard. Cracking experiments at 500 °C and contact times shorter than 3 s showed that the zeolite with the highest mesopore volume, derived from the parent one by desilication, was more active, particularly with the aromatic fraction. The improved activity was assigned to both the higher amount and accessibility of acidic sites after desilication.

The fractions had different reactivities, group yields being

dissimilar, as related to the nature of the feedstocks. Independent from the feedstock fraction, gasoline was the most important product, selectivities being as high as 60–70% at about 11% conversion. The reactivity of VGO over both zeolites differed from that of fraction SF, even though it was the major fraction (68%). This behavior could be the consequence of interactions between the various fractions composing VGO.

It was found that coke yield was favored by the increased mesoporosity in the modified zeolite, which allows accommodating coke precursors more easily and favoring reactions leading to the formation of carbonaceous deposits. However, independent from the feedstock, the desilicated zeolite kept its higher activity, thus showing to be more resistant to coke deactivation.

As expected, both textural and acidic properties in the zeolites were affected by coke deposition. Pore volume was particularly affected among physical properties, decreasing up to 38% in some cases, despite the low conversions. The modified zeolite (Y-10-S) was less affected than the parent zeolite, a fact that was assigned to increased interconnectivity in mesopores, improving the diffusion of bulky coke precursor molecules out of the zeolite structure. The loss of acidity was always very large, above 40%, the saturated fraction being the one with the lowest impact on this property.

The coke combustion profiles and the FTIR bands indicated that independent from the feedstocks two different natures aromatic and olefinic were always observed on coke formed over both zeolites. Olefinic coke was more abundant in the parent zeolite and aromatic coke prevailed in the modified zeolite, indicating that the nature of the coke depended not only on the feedstock, but also on zeolite properties.

Given the possibility of achieving extremely short contact times in a fluidized catalyst bed, allowing for small amounts of coke on catalyst, the CREC Riser Simulator reactor is a proper laboratory tool for this type of studies.

Acknowledgements

The financial support of Universidad Nacional del Litoral (Project CAID 2011 #50120110100546) and CONICET (PIP 593/13) is gratefully acknowledged.

References

[1] Chunming X, Jinsen G, Suoqi Z, Shixiong L. Fuel 2005;84:669–74.
[2] Speight J. The chemistry and technology of petroleum. 5th ed. Boca Raton: CRC Press-Taylor & Francis Group; 2014.
[3] Ancheyta J, Lopéz F, Aguilar E. Ind Eng Chem Res 1998;37:4637–40.
[4] Sadrameli SM. Fuel 2016;173:285–97.
[5] Lappas A, Patiaka D, Dimitriadis B, Vasalos I. Appl Catal A 1997;152:7–26.
[6] Sanchez F, Ancheyta J, Silva-Oliver G, Flores-Valle S. Fuel 2013;110:318–21.
[7] Fan T, Buckley J. Energy Fuels 2002;16:1571–5.
[8] Florez MA, Guerrero J, Cabanzo R, Mejía-Ospino E. J Petrol Sci Eng 2017;156:966–70.
[9] Kharrat A, Zacharia J, Cherian V, Anyatonwu A. Energy Fuels 2007;21:3618–21.
[10] Boysen RB, Schabron JF. Energy Fuels 2013;27:4654–61.
[11] Cumming KA, Wojciechowski BW. Catal Rev Sci Eng 1996;38:101–57.
[12] Al-Khattaf S, de Lasa H. Appl Catal A 2002;226:139–53.
[13] Martinez C, Verboekend D, Pérez-Ramírez J, Corma A. Catal Sci Technol 2012;3:972–81.
[14] García JR, Falco M, Sedran U. Top Catal 2016;59:268–77.
[15] Gayubo A, Alonso A, Valle B, Aguayo A, Bilbao J. Appl Catal B 2010;97:299–306.
[16] García-Martínez J, Johnson M, Valla J, Li K, Ying J. Catal Sci Technol 2012;2:987–94.
[17] Na K, Choi M, Ryoo R. Microporous Mesoporous Mater 2013;166:3–19.
[18] Kyungho L, Songhyun L, Youngsun J, Minkee C. J Catal 2017;347:222–30.
[19] García JR, Falco M, Sedran U. Catal Today 2017;296:247–53.
[20] Forzatti P, Lietti L. Catal Today 1999;52:165–81.
[21] Cerqueira H, Caeiro G, Costa L, Ramôa Ribeiro F. J Mol Catal A: Chem 2008;292:1–13.
[22] Cerqueira H, Ayrault P, Datka J, Magnoux P, Guisnet M. J Catal 2000;196:149–56.
[23] Baia D, Zhub J-X, Jina Y, Yua Z. Chem 1998;71:97–109.
[24] Ibarra A, Veloso A, Bilbao J, Arandes J, Castaño P. Appl Catal B 2016;182:336–46.
[25] Scherzer J. Catal Rev Sci Eng 1989;31:215–354.
[26] ASTM. Standard test method for characteristic groups in rubber extender and processing oils and other petroleum-derived oils by the clay-gel absorption chromatographic method. ASTM international 2016: D2007-11.
[27] de Jong K, Zečević J, Friedrich H, de Jongh P, Bulut M, van Donk S, et al. Angew Chem Int Ed 2010;49:10074–8.
[28] García JR, Bertero M, Falco M, Sedran U. Appl Catal A 2015;503:1–8.
[29] Rac V, Rakic V, Stošic C, Otman O, Auroux A. Microporous Mesoporous Mater 2014;194:126–34.
[30] Aguayo A, Castaño P, Mier D, Gayubo A, Olazar M, Bilbao J. Ind Eng Chem Res 2011;50:9980–8.
[31] Castaño P, Elordi G, Olazar M, Bilbao J. Chem Cat Chem 2012;4:631–5.
[32] Emeis C. J Catal 1993;141:347–54.
[33] Jorik V. Zeolites 1993;13:187–91.
[34] de Lasa H. Novel Riser Simulator reactor. US Patent 5.102.628, 1992.
[35] Gilbert W, Morgado E, de Abreu M, de la Puente G, Passamonti F, Sedran U. Fuel Process Technol 2011;92:2235–40.
[36] de Lasa H, Kraemer D. Novel techniques for FCC catalyst selection and kinetic modelling. In: de Lasa H, Doğu G, Ravella A, editors, Chemical reactor technology for environmentally safe reactors and products (NATO ASI Series E-Vol. 225), Kluwer Academic Publishers. Dordrecht 1993:71–131.
[37] Passamonti F, de La Puente G, Gilbert W, Morgado E, Sedran U. Zeolites 1993;13:187–91.
[38] Verboekend D, Vilé G, Pérez-Ramírez J. Adv Funct Mater 2012;22:916–28.
[39] Johnson M. J Catal 1978;52:425–31.
[40] Holm MS, Svelle S, Joensen F, Beato P, Christensen CH, Bordiga S. Appl Catal A General 2009;356:23–30.
[41] Wang D, Zhang L, Chen L, Wu H, Wu P. J Mater Chem A 2015;3:3511.
[42] Jiménez-García G, Aguilar-López R, Maya-Yescas R. Fuel 2011;90:3531–41.
[43] Pujro R, Falco M, Devard A, Sedran U. Fuel 2014;119:219–25.
[44] Mariaca-Domínguez E, Rodríguez-Salomón S, Maya-Yescas R. Int J Chem React Eng 2003;1:article A46.
[45] Stratiev D, Galkin V, Shishkova I, Minkov D, Stanulov K. Chem Technol Fuels Oils 2007;43:311–8.
[46] León-Becerril E, Maya-Yescas R, Salazar-Sotelo D. Chem Eng J 2004;100:181–6.
[47] Park H, Heo H, Jeon J, Kim J, Ryoo R, Jeong K, et al. Appl Catal B Environ 2010;95:365–73.
[48] Foster A, Jae J, Cheng Y, Huber G, Lobo R. Appl Catal A General 2012;423:154–61.
[49] Choi M, Na K, Kim J, Sakamoto Y, Terasaki O, Ryoo R. Nature 2009;461:246.
[50] Mochizuki H, Yokoi T, Imai H, Namba S, Kondo JN, Tatsumi T. Appl Catal A General 2012;449:188–97.
[51] Guisnet M, Magnoux P. Appl Catal A General 2001;212:83–96.
[52] Bauer F, Karge HG. Mol Siev 2007;5:249–364.
[53] Zhang H, Shao S, Xiao R, Shen D, Zeng J. Energy Fuels 2014;28:52–7.
[54] Sadeghbeigi R. Fluid catalytic cracking handbook. 3rd ed. Oxford: Butterworth-Heinemann; 2012.
[55] Ribeiro FR, Alvarez F, Henriques C, Lemos F, Lopes JM, Ribeiro MF. J Mol Catal A Chem 1995;96:245–70.
[56] Katada N, Suzuki K, Noda T, Miyatani W, Taniguchi F, Niwa M. Appl Catal A General 2010;373:208–13.
[57] Wang CM, Brogaard RY, Weckhuysen BM, Nørskov JK, Studt F. J Phys Chem Lett 2014;5:1516–21.
[58] Jacobs P, Heylen C. J Catal 1974;34:267–74.